coatings

MDPI

Article

Novel Effect of Post-Oxidation on the Comprehensive Performance of Plasma Nitriding Layer

Jia Ni [1], Heng Ma [1], Wei Wei [1,2], Xulong An [1,2], Minhua Yu [3] and Jing Hu [1,3,*]

[1] Jiangsu Key Laboratory of Materials Surface Science and Technology, National Experimental Demonstration Center for Materials Science and Engineering, Changzhou University, Changzhou 213164, China; 15861193706@163.com (J.N.)
[2] Huaide College, Changzhou University, Jingjiang 214500, China
[3] Department of Integrated Management, Jiangsu Shuangliang Boiler Co., Ltd., Jiangyin 214444, China
* Correspondence: jinghoo@126.com; Tel.: +86-0519-8633-0095

Abstract: In order to enhance the comprehensive performance of plasma nitrided heavy load components used in corrosive environments, post-oxidation was conducted under different conditions after plasma nitriding 42CrMo4 steel at 500 °C for 5 h. The results show that an oxide film composed of Fe_3O_4 and Fe_2O_3 was formed above the compound layer, resulting in a significant increase in corrosion resistance; the self-corrosion potential was greatly increased from −658.72 mV to −429.23 mV. Meanwhile, it needs to be emphasized that the characteristics of the plasma nitriding layer could be effectively adjusted as expected by post-oxidation. The compound layer thickness decreased from 9.41 μm to 3.62 μm by post-oxidation at 400 °C for 2 h, while the thickness of the effective hardening layer increased from 300 μm to 378 μm. Due to the expected change in the characteristics of the plasma nitriding layer, post-oxidation could simultaneously improve the toughness, hardness, and wear resistance of the samples; the brittleness level decreased from Grade 4 to Grade 1; the surface hardness increased from 765 $HV_{0.05}$ to 825 $HV_{0.05}$; and the wear rate decreased from 3×10^{-5} $g \cdot m^{-1} \cdot N^{-1}$ to 1.19×10^{-5} $g \cdot m^{-1} \cdot N^{-1}$, illustrating that the wear resistance was greatly improved.

Keywords: plasma nitriding; post-oxidation; hardness; toughness; wear resistance

Citation: Ni, J.; Ma, H.; Wei, W.; An, X.; Yu, M.; Hu, J. Novel Effect of Post-Oxidation on the Comprehensive Performance of Plasma Nitriding Layer. *Coatings* **2024**, *14*, 86. https://doi.org/10.3390/coatings14010086

Academic Editor: Alessandro Patelli

Received: 27 November 2023
Revised: 3 January 2024
Accepted: 4 January 2024
Published: 8 January 2024

1. Introduction

Heavy load components are widely used in aviation, automobile, rail transit, and other corrosive environments; hence, excellent wear and corrosion resistance and appropriate toughness are needed as they are applied in harsh environments [1]. In order to meet the technical requirements of the heavy load components, surface modification is necessary to improve the comprehensive properties. The commonly used surface heat treatment processes for heavy-load components include carburizing and quenching, induction hardening, and nitriding.

After carburizing and quenching treatment, the components can obtain a deeper hardened layer and higher fatigue strength. Unfortunately, the carburizing process has high energy consumption as it is generally conducted at temperatures above 900 °C. Moreover, it is difficult to overcome the severe distortion throughout the process [2].

Though induction hardening has the advantages of high production efficiency, energy saving, low environmental pollution, and easy automation, certain problems exist, including lower tooth surface hardness and shallow hardening layer depth. The residual compressive stress on the tooth surface and the residual tensile stress on the tooth root increase susceptibility to bending fatigue fracture [3].

Compared with carburizing and induction hardening, the surface layer treated by nitriding has higher hardness and better wear and fatigue resistance [4–9]. Meanwhile, nitriding causes minimal distortion due to treatment at a lower temperature. Therefore, it is widely used in steel components, such as automotive gears, crankshafts, molds, and tools.

Plasma nitriding (PN) is a popular nitriding technology that is environment-friendly, providing efficient surface modification [10–13] to improve the wear resistance of components by forming a nitrided layer [14–18]. Generally, a nitrided layer is composed of a top compound layer and a bottom diffusion layer [19]. Since the compound layer is hard and brittle [20–25]. Thus, collaborative deformation does not readily occur with the diffusion layer. Therefore, a thick compound layer has a strong tendency to crack when subjected to severe impacts and heavy loads, such as heavy-load gears and impact molds. From this perspective, it is evident that a thick compound layer must be avoided for components subjected to severe impact and heavy load wear to prevent premature crack failure.

In real applications, a thin compound layer is generally obtained by decreasing the nitriding temperature and time or decreasing the ratio of nitrogen to hydrogen [26]. Unfortunately, a thin compound layer formed by the reported methods is generally accompanied by a thin, hardening layer, which results in a lower surface hardness and poorer wear resistance than that with a thick nitrided layer, making it difficult to meet the long service life requirements of components subjected to severe impact and heavy load wear, though premature cracking can be avoided.

Therefore, it is of great value to develop a novel method comprising a nitriding layer with a thin, brittle compound layer and a thick diffusion layer for components subjected to severe impact and heavy load wear. In our previous research [27–30], post-oxidation (PO) could adjust the characteristics of the nitriding layer, i.e., change the ratio of the compound layer thickness to the diffusion layer thickness. However, no studies have reported on the effect of PO on the nitrided layer toughness.

Thus, in this study, post-oxidation (PO) is proposed to enhance the comprehensive performance of the plasma nitriding layer and enhance the toughness of the components without sacrificing the hardness and wear resistance. From the perspective of engineering applications, this research is highly important for components subjected to severe impact and heavy load wear.

2. Experimental

42CrMo4 steel in the quenched and tempered state was used in this study. The samples were processed to 15 mm × 15 mm × 10 mm. The mechanically polished samples were prepared with different granulometries of SiC papers (180#~2000#) and washed in anhydrous ethanol with ultrasonic application for 10 min.

The samples were divided into two groups: one was subjected to plasma nitriding (PN) at 500 °C for 5 h, and the other was subjected to post-oxidation (PO) under different conditions after the same PN process. The PO conditions were 350 °C for 1 h, 400 °C for 1 h, 450 °C for 1 h, 400 °C for 2 h, and 400 °C for 4 h. Each process was repeated 3 times. The process flow of plasma nitriding and post-oxidation is shown in Figure 1.

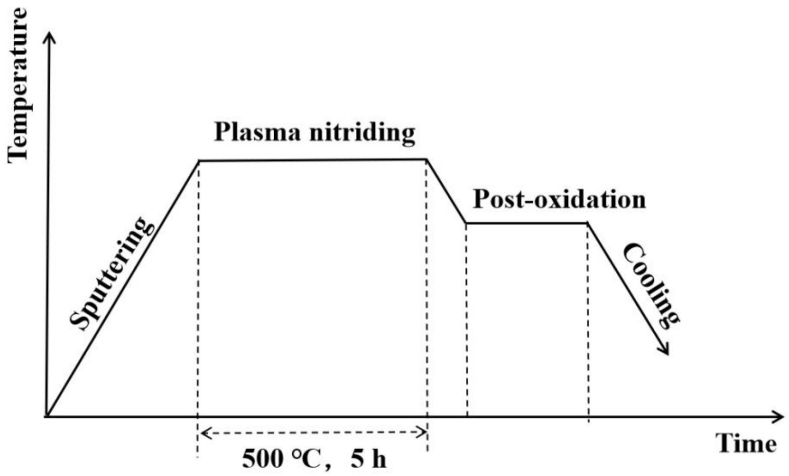

Figure 1. Process chart of plasma nitriding and post-oxidation.

After plasma treatment, the optical microscope (OM, DMI-3000M, Leica Microsystems, Shanghai, China) was used to observe the microstructure and measure the compound layer thickness. An X-ray diffractometer (XRD, D/MAX-2500, Rigaku Corporation, Tokyo, Japan) with Cu-Kα radiation was used to determine the phase composition. The Scanning Electron Microscope (SEM, ZEISS EVO 18, Carl Zeiss AG, Jena, Germany) was used to observe the cross-sectional structure. The Vickers microhardness tester (HXD-1000TMC, SRIM, Shanghai, China) was used to measure the surface hardness, and the brittleness level was determined according to the Chinese national standard [31] based on the cracking degree of indentation corners after Vickers hardness testing. The electrochemical workstation (CS350, Corrtest Instrument, Wuhan, China) was used to test the corrosion resistance. The wear test was carried out on the high-temperature friction (HT-600, Zhongke KaiHua Co., Ltd., Lanzhou, China), with the friction load set to 200 N, wear time set to 15 min, and a GCr15 steel ball with a 2-mm radius as the grinding material. To obtain an average value and error range, 5 microhardness tests and 3 wear and corrosion tests were performed for samples treated under the same plasma parameters. Finally, the wear tracks were observed by optical microscopy. An electronic balance was used to weigh the samples before and after the wear test. The weight-specific wear rate was calculated based on Equation (1):

$$W = \Delta M/(F \times S) \quad (1)$$

where W is the weight-specific wear rate, ΔM is the weight change before and after treatment, F is the test load, and S is the sliding distance of the ball.

3. Results

3.1. Sectional Microstructure and Compound Layer Thickness

Figure 2 shows the sectional microstructure of samples treated by PN and PO under different conditions. It can be seen from (a)–(d) that with an increase in the post-oxidation temperature, the thickness of the compound layer decreased from 9.41 μm to 4.89 μm. In addition, (e) and (f) show that the post-oxidation time had an obvious effect on thinning the compound layer. When the post-oxidation time was 2 h, the thinnest compound layer was obtained with a thickness of 3.62 μm. This result may be attributed to the decomposition of nitride in the compound layer by the oxygen ions constantly bombarding the surface during the PO process, leading to nitrogen ions forming and diffusing into the matrix, making the compound layer thinner.

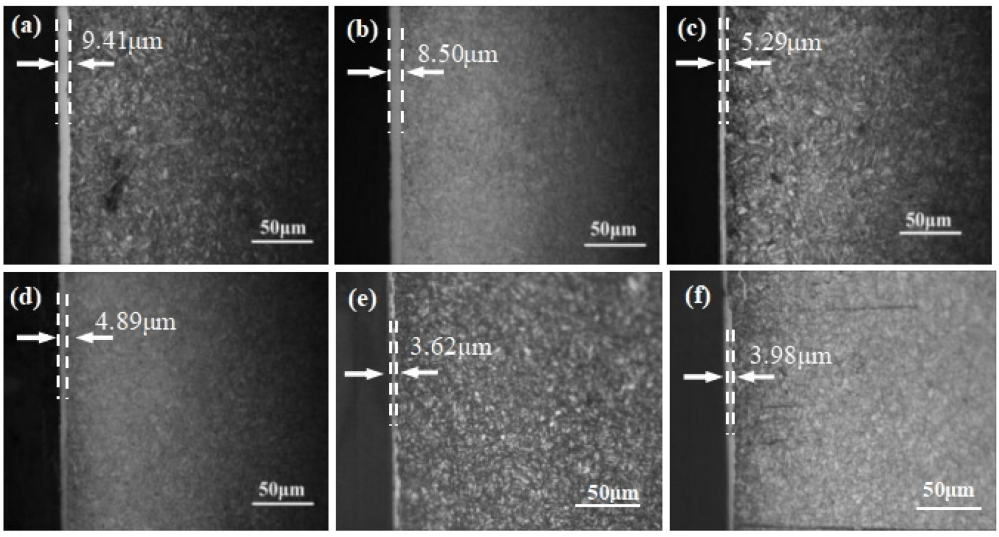

Figure 2. Microstructure of samples treated by PN with and without PO under different conditions. (**a**) PN only; (**b**) PO 350 °C for 1 h; (**c**) PO 400 °C for 1 h; (**d**) PO 450 °C for 1 h; (**e**) PO 400 °C for 2 h; (**f**) PO 400 °C for 4 h.

3.2. Phase Composition Analysis

The XRD sample patterns in Figure 3 show that the phase composition of the PN sample was mainly composed of γ′-Fe_4N and ε-$Fe_{2-3}N$ phases. While the γ′-Fe_4N and ε-$Fe_{2-3}N$ peaks were small, those of Fe_2O_3 and Fe_3O_4 were large for PO samples. The ratio of Fe_3O_4 to Fe_2O_3 was highest under 400 °C for 2 h PO conditions. This suggests that optimal corrosion resistance can be obtained under this PO condition.

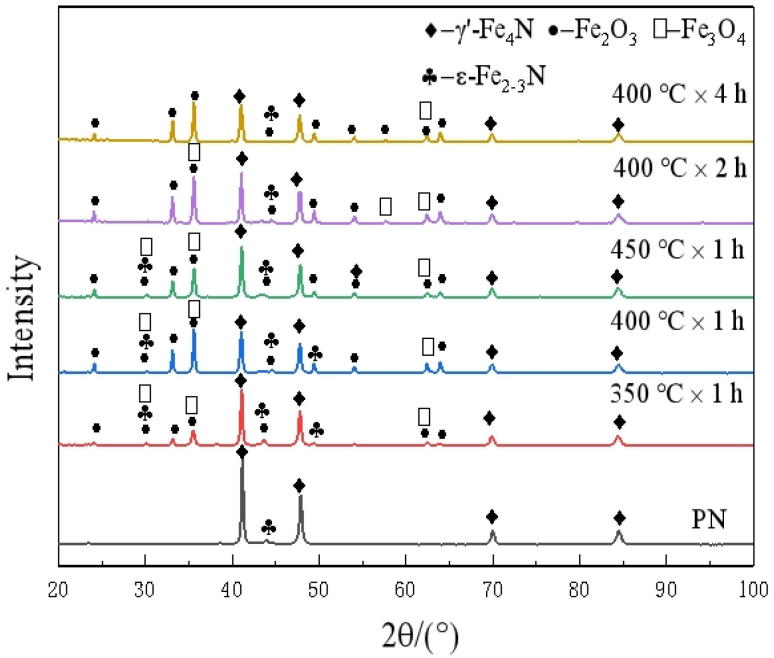

Figure 3. XRD patterns for samples treated by PN and PO under different conditions.

3.3. Sectional Microhardness Profile and Effective Hardening Layer Thickness

The effective hardening layer thickness corresponds to the vertical distance from the surface of the sample to 50 HV above the substrate hardness. The horizontal coordinate corresponding to the dashed line in Figure 4a is the effective hardening layer thickness under this condition. The cross-sectional microhardness profile of samples treated by PN and PO is presented in Figure 4a; the top surface layer hardness profile at higher magnification is presented in the embedded panel. Figure 4a clearly demonstrates that the surface hardness and the thickness of the effective hardening layer after PO were enhanced compared with the sample treated with only PN. The surface hardness of the sample increased from 765 $HV_{0.05}$ to a maximum of 825 $HV_{0.05}$; the thickness of the effective hardening layer increased from 300 μm to a maximum of 378 μm under the PO condition of 400 °C for 2 h. This is due primarily to the formation of active nitrogen atoms via nitride decomposition in the compound layer during the PO process. A portion of the active nitrogen atoms diffuse inward to the matrix, further improving the solid solution strengthening effect, leading to increased hardness and a thicker effective hardening layer. However, excessively high PO temperatures or long PO times result in nitride coarsening, causing the microhardness to decrease. In addition, it can be seen from Figure 4b that an oxide film was formed above the compound layer after PO treatment, resulting in the maximum hardness located at the subsurface layer instead of the top surface.

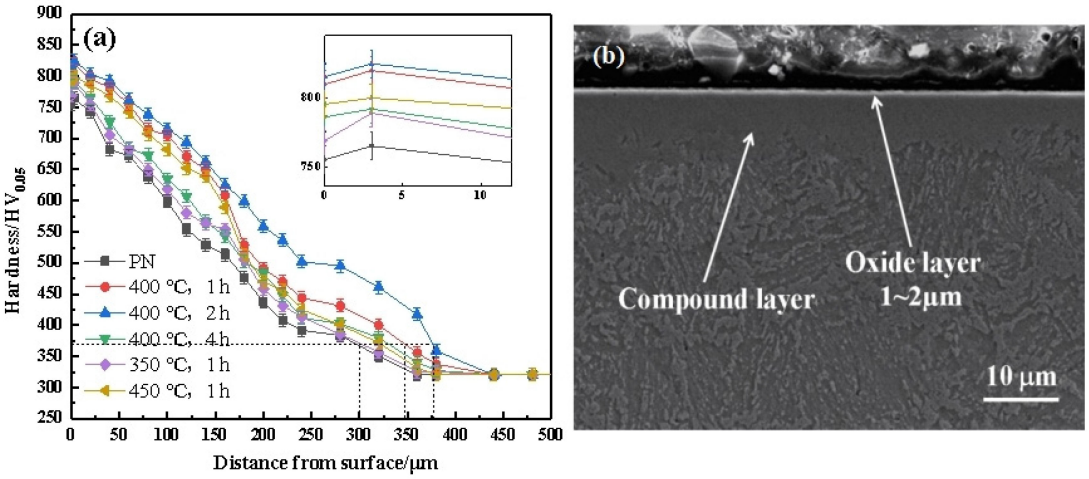

Figure 4. Sectional hardness profile and surface oxide layer observed by SEM. (**a**) Sectional hardness; (**b**) surface oxide layer observed by SEM.

3.4. Toughness Analysis

Generally, toughness represents the ability to absorb energy before cracking or fracturing; the more energy absorbed before cracking or fracture, the better the toughness. In other words, cracking more readily occurs under the same load when the toughness is low. According to the Chinese national standard [31], the brittleness grade of the nitriding layer is divided into five levels based on the indentation cracking degree after the Vickers hardness test, as shown in Table 1. The highest level is Grade 5, corresponding to the most severe cracking, appearing on four sides or corners; Grade 4 corresponds to cracking on three sides or corners; Grade 3 refers to cracking on two sides or corners; Grade 2 corresponds to cracking on one side or corner; and Grade 1 corresponds to no cracking around the indentation, representing the highest toughness.

Table 1. Description of nitriding layer brittleness grades.

Grade	Description of the Cracking Degree of Indentation after Vickers Hardness Test
1	Indentation corners intact
2	Indentation cracking on one side or corner
3	Indentation cracking on two sides or corners
4	Indentation cracking on three sides or corners
5	Indentation cracking on four sides or corners

The indentations of samples treated by PN and PO under different conditions are presented in Figure 5. Serious cracking is clearly visible on three sides around the indentation for the sample treated with PN only, with a Grade 4 brittleness level [31]. The cracking degree around the indentation for the sample after PO treatment was obviously reduced, and no cracking was observed around the indentation of the sample treated with PO at 400 °C for 2 h (Grade 1) [31]. Hence, PO can effectively decrease the brittleness grade and improve the toughness of samples, with Grade 1 brittleness and optimal toughness achieved under PO at 400 °C for 2 h. Meanwhile, the indentation area with PO was smaller than that with PN alone, implying that PO improves the surface hardness of the samples, consistent with the results shown in Figure 4.

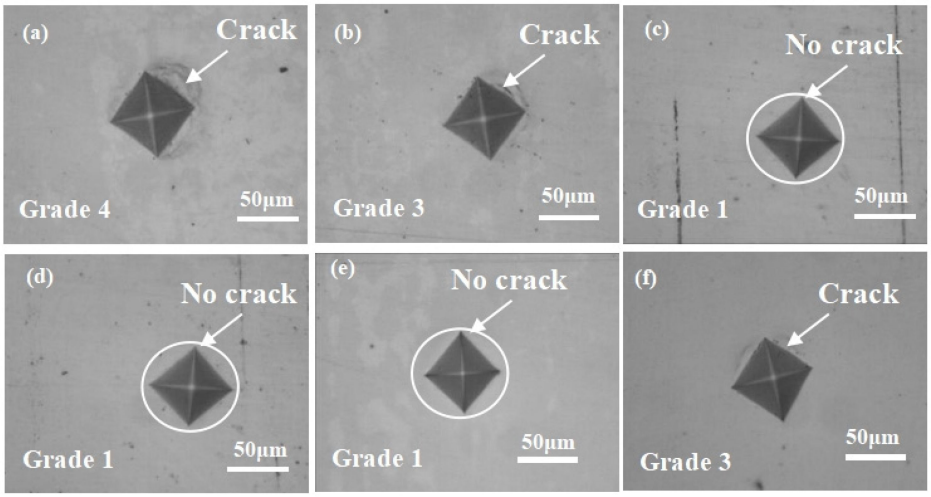

Figure 5. Indentation morphology for samples treated by PN with and without PO under different conditions. (**a**) PN only; (**b**) PO 350 °C for 1 h; (**c**) PO 400 °C for 1 h; (**d**) PO 450 °C for 1 h; (**e**) PO 400 °C for 2 h; (**f**) PO 400 °C for 4 h.

3.5. Wear Resistance Analysis

Figure 6 shows the wear track of samples treated by PN and PO. The wear path of the sample treated with only PN appeared wider, while the wear tracks of the samples treated with PN and PO were narrower. As can be seen from Figure 7, the wear rate decreased with PO treatment, reaching the minimum of 1.19×10^{-5} g·m^{-1}·N^{-1} following treatment with PO at 400 °C for 2 h. Therefore, the wear resistance of PN-ed samples is effectively improved by subsequent PO treatment [32].

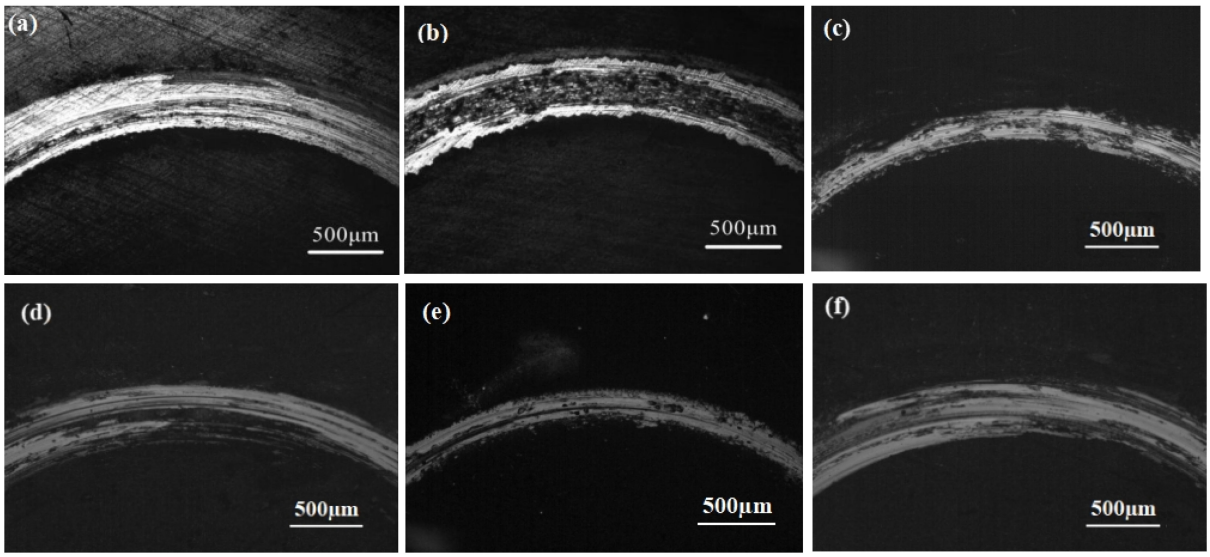

Figure 6. Wear track of samples treated by PN with and without PO under different conditions (**a**) PN only; (**b**) PO 350 °C for 1 h; (**c**) PO 400 °C for 1 h; (**d**) PO 450 °C for 1 h; (**e**) PO 400 °C for 2 h; (**f**) PO 400 °C for 4 h.

As can be seen, the γ′-Fe_4N and ε-$Fe_{2\text{-}3}N$ peaks are weaker during the PO process in Figure 3, indicating that iron nitrides were gradually decomposed during the PO process, making the compound layer thinner. Meanwhile, the decomposed active nitrogen atoms can diffuse into the matrix, thus improving the solid solution strength, resulting in increased hardness and effective hardening of the layer, Therefore, the wear resistance can be enhanced.

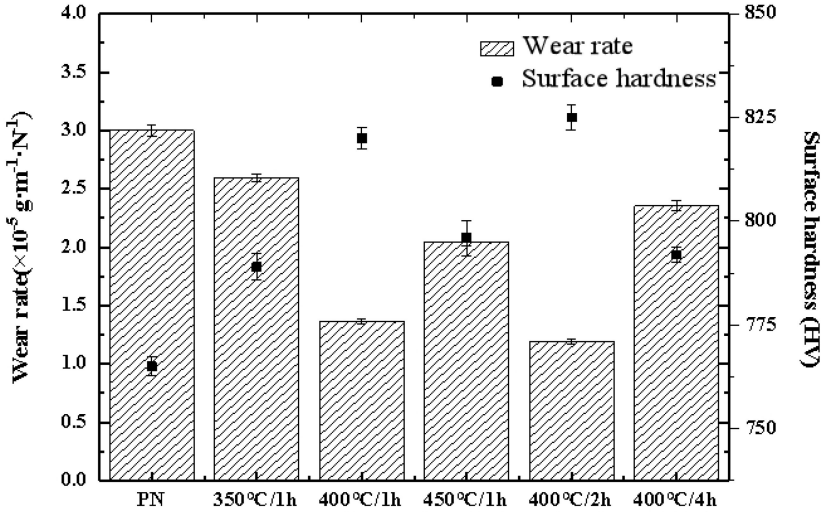

Figure 7. Wear rate of samples treated by PN and PO.

3.6. Corrosion Resistance Analysis

Figure 8 shows the polarization curve of samples treated by PN and PO. The self-corrosion potential and self-corrosion current of PN samples were −658.72 mV and 1.2010×10^{-5} A/cm^2, respectively, while the self-corrosion potential peaked at −429.23 mV and the self-corrosion current decreased to 1.0508×10^{-6} A/cm^2 after PO treatment at 400 °C for 2 h. It can be concluded that the corrosion resistance of the PN sample is greatly improved by PO, attributed to the formation of an oxide film composed of Fe_3O_4 and Fe_2O_3 above the compound layer, as shown in Figures 3 and 4.

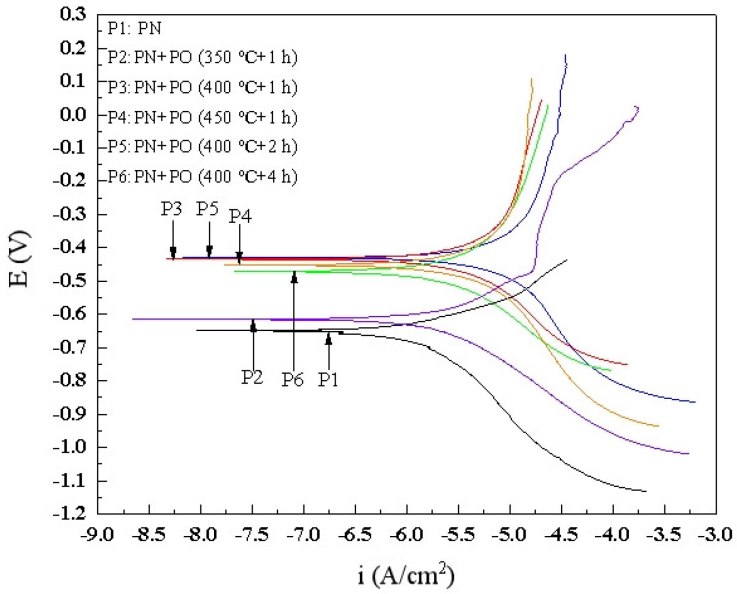

Figure 8. Corrosion resistance of samples treated by PN and PO.

4. Discussions

To summarize the above results, the characteristics and properties of the nitriding layers formed by PN with and without subsequent PO are presented in Table 2.

As can be seen from Figure 3, Fe_2O_3 and Fe_3O_4 iron oxides appear in the XRD patterns of the samples after PO treatment. Combined with the oxidized surface morphology in Figure 4b, it can be concluded that an oxide layer is generated above the nitriding layer during PO treatment.

Table 2. Characteristics and comprehensive properties of samples treated by PN with and without PO.

Treatment Process	Compound Layer/μm	Effective Hardening Layer/μm	Maximum Hardness /$HV_{0.05}$	Brittleness Grade	Wear Rate/ $g \cdot m^{-1} \cdot N^{-1}$	Corrosion Resistance	
						Ecorr (mV)	Icorr ($\times 10^{-6}$ A/cm^2)
PN (without PO)	9.41	300	765	4	3	−658.72	12.010
PN + PO (350 °C × 1 h)	8.50	323	789	3	2.59	−628.12	10.197
PN + PO (400 °C × 1 h)	5.29	347	820	1	1.36	−433.98	3.8966
PN + PO (450 °C × 1 h)	4.89	331	796	1	2.04	−455.79	4.2463
PN + PO (400 °C × 2 h)	3.62	378	825	1	1.19	−429.23	1.0508
PN + PO (400 °C × 4 h)	5.06	340	792	3	2.35	−470.57	6.4040

Meanwhile, Table 2 shows that the thickness of the compound layer decreases and the effective hardening layer increases, implying that decomposition of iron nitrides occurs and a stronger nitrogen solution strengthening effect appears during the PO process.

To explain the above phenomena and results, the following reactions are proposed to occur during the PO process [33,34]:

$$2Fe_xN + xO_2 \rightarrow 2xFeO + 2[N] \quad (2)$$

$$6FeO + O_2 \rightarrow 2Fe_3O_4 \quad (3)$$

$$Fe_3O_4 + 4H_2 \rightarrow 3Fe + 4H_2O \quad (4)$$

$$3Fe + 2O_2 \rightarrow Fe_3O_4 \quad (5)$$

$$4Fe + 3O_2 \rightarrow 2Fe_2O_3 \quad (6)$$

$$4Fe_3O_4 + O_2 \rightarrow 6Fe_2O_3 \quad (7)$$

Equations (2)–(4) illustrate the decomposition of iron nitrides. The top loose nitriding layer is decomposed preferentially, which is beneficial to increase the surface hardness and improve the toughness, enhancing the wear resistance for heavy load components.

In addition, the decomposed nitrogen atoms can diffuse inward, thus further improving the solution-strengthening effect, resulting in an increase in the effective hardening layer depth.

Equations (5)–(7) illustrate the formation of iron oxides during PO treatment under appropriate PO conditions of 400 °C for 2 h, resulting in a maximum Fe_3O_4 to Fe_2O_3 ratio and optimal overall performance [33,34].

5. Conclusions

(1) Post-oxidation (PO) was primarily used to enhance the comprehensive properties of heavy load components, which can enhance the wear resistance and the toughness of the nitrided layer by making the compound layer thinner and the diffusion layer thicker. Thus it holds great application value.

(2) The thickness of the compound layer decreased from 9.41 μm to 3.62 μm, while the thickness of the effective hardening layer increased from 300 μm to 378 μm by PO at 400 °C for 2 h.

(3) PO simultaneously improved the toughness, hardness, wear resistance, and corrosion resistance of the samples. The optimal comprehensive performance could be obtained by PO at 400 °C for 2 h, with the highest surface hardness of 825 $HV_{0.05}$, lowest brittleness level of Grade 1, lowest wear rate of 1.19×10^{-5} $g \cdot m^{-1} \cdot N^{-1}$, and maximum self-corrosion potential of −429.23 mV.

(4) An oxidation layer mainly composed of Fe_3O_4 and Fe_2O_3 was formed by PO. The Fe_3O_4 phase reached the maximum value by PO at 400 °C for 2 h. Meanwhile, the γ′-Fe_4N and ε-$Fe_{2\text{-}3}N$ phase diffraction peaks markedly decreased.

Author Contributions: J.N.: conceptualization, methodology, experiments, writing—original draft preparation. H.M.: visualization, investigation. M.Y.: software, validation. W.W.: investigation. X.A.: experiment assistant. J.H.: supervisor, writing—reviewing and editing. All authors have read and agreed to the published version of the manuscript.

Funding: This research was supported by the National Natural Science Foundation of China (21978025), PAPD-3 and TAPP.

Institutional Review Board Statement: Not applicable.

Informed Consent Statement: Not applicable.

Data Availability Statement: The data presented in this study are available on request from the corresponding author.

Conflicts of Interest: Minhua Yu and Jing Hu were employed by the company Jiangsu Shuangliang Boiler Co., Ltd. The remaining authors declare that the research was conducted in the absence of any commercial or financial relationships that could be construed as a potential conflict of interest.

References

1. Wang, Z.Y.; Xing, Z.G.; Wang, H.D.; Li, G.L.; Liu, K.J.; Xing, Z. Research status of test method for bending fatigue life of heavy duty gear. *Mater. Rev.* **2018**, *32*, 3051–3059.
2. Li, B.K.; Wang, A.X.; Gu, M. Research status on distortion control of carburizing and hardening gears. *Heat. Treat. Met.* **2006**, *31*, 6–11.
3. Lu, J.S.; Li, B.K. Discussion of precision heat treatment and anti-fatigue manufacturing of gear. *J. Mech. Eng.* **2019**, *43*, 170–175.
4. Li, J.; Tao, X.; Wu, W.; Xie, G.; Yang, Y.; Zhou, X.; Zhang, S. Effect of arc current on the microstructure, tribological and corrosion performances of AISI 420 martensitic stainless steel treated by arc discharge plasma nitriding. *J. Mater. Sci.* **2023**, *58*, 2294–2309. [CrossRef]
5. Hong, H.; Xie, G.; Sun, L.; Yang, Y.; Zhang, Z.; Li, J.; Zhang, S. The diffusion behavior and surface properties of catalytic nitriding with LaFeO3 film prepared by the sol-gel method. *Surf. Coat. Technol.* **2023**, *467*, 129720. [CrossRef]
6. Du, C.; Zhang, J.; Zhang, L.; Lian, Y.; Fang, M. Acceleration effects of rare earths on salt bath nitriding: Diffusion kinetics and first-principles calculations. *Surf. Eng.* **2021**, *37*, 764–774. [CrossRef]
7. Shi, T.; Sun, J.Q.; Wang, X.W.; He, Q.K.; Si, J.W.; Wang, D.R.; Xie, K.; Li, W.S. Effect of trace water in ammonia on breaking passive film of stainless steel during gas nitriding. *Vacuum.* **2022**, *202*, 111216. [CrossRef]
8. Liu, R.L.; Yan, F.Y.; Yan, M.F. Surface grain nanocrystallization of Fe-Cr-Ni alloy steel by plasma thermochemical treatment. *Surf. Coat. Technol.* **2019**, *370*, 136–143. [CrossRef]
9. Samal, S.; Cibulková, J.; Čtvrtlík, R.; Tomáštík, J.; Václavek, L.; Kopeček, J.; Šittner, P. Tribological Behavior of NiTi Alloy Produced by Spark Plasma Sintering Method. *Coatings* **2021**, *11*, 10. [CrossRef]
10. Men, S.W.; Xie, J.M.; Liu, X.; Yang, Y.; Yang, K.; Zhang, S.H. A novel crack healing in sprayed FeCrBSi coatings by plasma nitriding. *Vacuum.* **2023**, *209*, 111768. [CrossRef]
11. Li, J.; Men, S.W.; Zhang, Z.; Yang, Y.; Sun, Y.; Ding, J.C.; Wang, Q.M. Structural, mechanical, and tribological properties of GLC film on a nitrided layer prepared in a glow-discharge plasma nitriding system. *Vacuum.* **2021**, *193*, 110543. [CrossRef]
12. Sun, J.; Li, J.; Xie, J.M.; Yang, Y.; Wu, W.P.; Zhou, X.; Zhang, S.H.; Wang, Q.M. Properties of rapid arc discharge plasma nitriding of AISI 420 martensitic stainless: Effect of nitriding temperatures. *J. Mater. Res. Technol.* **2022**, *19*, 4804–4814. [CrossRef]
13. Li, L.; Liu, R.; Liu, Q.; Wu, Z.; Meng, X.; Fang, Y. Effects of Initial Microstructure on the Low-Temperature Plasma Nitriding of Ferritic Stainless Steel. *Coatings* **2022**, *12*, 1404. [CrossRef]
14. Li, Y.; Wang, L.; Zhang, D.; Shen, L. Improvement of corrosion resistance of nitrided low alloy steel by plasma post-oxidation. *Appl. Surf. Sci.* **2010**, *256*, 4149–4152. [CrossRef]
15. Yan, M.F.; Wang, X.A.; Liu, R.L.; Zhang, Y.X.; Yang, Y. Kinetics and wear behavior of M50NiL steel plasma nitrided at low temperature. *Mater. Sci. Tech-Lond.* **2016**, *33*, 370–376. [CrossRef]
16. Liu, R.L.; Yan, M.F. Characteristics of AISI 420 Stainless Steel Modified by Low-Temperature Plasma Carburizing with Gaseous Acetone. *Coatings* **2019**, *9*, 75. [CrossRef]
17. Yan, M.F.; Wu, Y.Q.; Liu, R.L.; Yang, M.; Tang, L.N. Microstructure and mechanical properties of the modified layer obtained by low temperature plasma nitriding of nanocrystallized 18Ni maraging steel. *Mater. Des.* **2013**, *47*, 575–580. [CrossRef]
18. Yan, M.F.; Chen, B.F.; Li, B. Microstructure and mechanical properties from an attractive combination of plasma nitriding and secondary hardening of M50 steel. *Appl. Surf. Sci.* **2018**, *455*, 1–7. [CrossRef]
19. Yan, M.F.; Wu, Y.Q.; Liu, R.L. Grain and grain boundary characters in surface layer of untreated and plasma nitrocarburized 18Ni maraging steel with nanocrystalline. *Appl. Surf. Sci.* **2013**, *273*, 520–526. [CrossRef]
20. Wang, B.; Liu, B.; Zhang, X.; Gu, J. Enhancing heavy load wear resistance of AISI 4140 steel through the formation of a severely deformed compound-free nitrided surface layer. *Surf. Coat. Technol.* **2018**, *356*, 89–95. [CrossRef]

21. Kim, Y.M.; Son, S.W.; Lee, W.B. Thermodynamic and kinetic analysis of formation of compound layer during gas nitriding of AISI1018 carbon steel. *Met. Mater. Int.* **2018**, *24*, 180–186. [CrossRef]
22. Saeed, A.; Khan, A.W.; Jan, F.; Shah, H.U.; Abrar, M.; Zaka-Ul-Islam, M.; Khalid, M.; Zakaullah, M. Optimization study of pulsed DC nitrogen-hydrogen plasma in the presence of an active screen cage. *Plasma Sci. Technol.* **2014**, *16*, 460–464. [CrossRef]
23. Ma, H.; Wei, K.; Zhao, X.; Liu, X.; Hu, J. Performance enhancement by novel plasma boron-nitriding for 42CrMo4 steel. *Mater. Lett.* **2021**, *304*, 130709. [CrossRef]
24. Nishimoto, A.; Nagatsuka, K.; Narita, R.; Nii, H.; Akamatsu, K. Effect of the distance between screen and sample on active screen plasma nitriding properties. *Surf. Coat. Technol.* **2010**, *205*, S365–S368. [CrossRef]
25. Tang, L.; Jia, W.; Hu, J. An enhanced rapid plasma nitriding by laser shock peening. *Mater. Lett.* **2018**, *231*, 91–93. [CrossRef]
26. Peng, T.; Zhao, X.; Chen, Y.; Tang, L.; Wei, K.; Hu, J. Improvement of stamping performance of H13 steel by compound-layer free plasma nitriding. *Surf. Eng.* **2020**, *36*, 492–497. [CrossRef]
27. Shen, H.Y.; Wang, L. Oxide layer formed on AISI 5140 steel by plasma nitriding and post-oxidation in a mixture of air and ammonia. *J. Alloys Compd.* **2019**, *806*, 1517–1521. [CrossRef]
28. Alsaran, A.; Altun, H.; Karakan, M.; Çelik, A. Effect of post-oxidizing on tribological and corrosion behaviour of plasma nitrided AISI 5140 steel. *Surf. Coat. Technol.* **2004**, *176*, 344–348. [CrossRef]
29. Prakash, N.A.; Bennett, C.J. The effect of plasma nitriding and post oxidation on fretting wear behaviour of a high strength alloy steel. *J. Phys. Conf. Ser.* **2017**, *843*, 012079. [CrossRef]
30. Zhang, L.; Ren, C.; Yu, Q.; Zhang, J.; Sun, S.; Ren, Q.; Lian, Y.; Chen, X.; Gao, W. Microstructure and properties of 1Cr12Ni2WMoVNb (GX-8) steel bored barrels with and without QPQ treatment. *Surf. Coat. Technol.* **2017**, *315*, 95–104. [CrossRef]
31. *GB/T 11354-2005*; Determination of Nitrided Case Depth and Metallographic Microstructure Examination for Steel and Iron Parts. Standardization Administration of China: Beijing, China, 2005.
32. Sun, J.; Wang, D.; Yang, J.; Li, F.; Zuo, L.; Ge, F.; Chen, Y. In Situ Preparation of Nano-Cu/Microalloyed Gradient Coating with Improved Antifriction Properties. *Coatings* **2022**, *12*, 1336. [CrossRef]
33. Wu, J.Q.; Mao, C.J.; Wei, K.X.; Hu, J. Titanium-modified plasma nitriding layer and enhanced properties for 42CrMo steel. *J. Mater. Res. Technol.* **2022**, *18*, 3819–3825. [CrossRef]
34. Wu, J.Q.; Li, H.; Li, J.C.; Hu, J. Post-oxidation treatments of plasma nitrided 42CrMo steel. *Trans. Mater. Heat Treat.* **2015**, *36*, 78–82.